Scattering-matrix treatment of patterned multilayer photonic structures

D. M. Whittaker
Toshiba Research Europe Limited, 260 Cambridge Science Park, Cambridge CB4 0WE, United Kingdom

I. S. Culshaw
Department of Physics and Astronomy, University of Sheffield, Sheffield S3 7RH, United Kingdom
(Received 18 February 1999)

We present calculations of surface reflectivity and emission spectra for multilayer dielectric waveguides with a two-dimensional patterning of deep holes. The spectra are obtained using a scattering-matrix treatment to propagate electromagnetic waves through the structure. This treatment incorporates, in a natural way, the extended boundary conditions necessary to describe external reflection and emission processes. The calculated spectra demonstrate how such measurements can be used to obtain experimental information about the waveguide photonic band structure, the coupling of scattering modes to external fields, and the field distribution within the waveguide. [S0163-1829(99)15327-X]

I. INTRODUCTION

Patterning a semiconductor waveguide with a lattice of holes is an important way of realizing the concept of a two-dimensional photonic band structure.[1] However, the realization is only approximate, as the waveguide provides additional optical confinement in the third dimension, perpendicular to the plane of the patterning. For a realistic semiconductor waveguide structure, which consists of a number of layers with different dielectric constants, the resulting electromagnetic modes are more complicated than in a simple two-dimensional lattice. Moreover, many, and sometimes all, the waveguide modes are actually scattering states, in that they can leak either out of the surface or into the substrate. This complicates the theoretical analysis of such structures, as the external coupling has to be taken into account.

The methods described in this paper provide a means to solve Maxwell's equations for a realistic patterned multilayer structure with external coupling, and so for calculating reflectivity and emission spectra. The motivation for developing this treatment was an experimental study of angular-dependent surface reflectivity measurements by Astratov *et al.*[2] These experiments provided much more detailed information about the photonic band structure than the in-plane propagation measurements of Ref. 1. Illuminating at a particular angle of incidence picks out a definite value of the in-plane photon wave vector; the various photonic bands for this wave vector then appear as sharp resonances in the reflectivity spectra. Thus, angular-dependent measurements can be used to map out the waveguide band structure of the scattering modes, and determine the strength of their external coupling. Comparisons between these experiments and the present theory are discussed in Ref. 2; the main purpose of this paper is to describe the theoretical treatment.

There have been many studies of two-dimensional band structures,[3] including the reflectivity of surfaces perpendicular to the plane of propagation.[4] Treatments of waveguides are much fewer: Atkin *et al.*[5] and Charlton *et al.*[6] have discussed the conditions for the formation of true guided (that is, not scattering) modes. However, it is the scattering modes, and how they couple to external fields, that are of interest here. Fan *et al.*[7] have tackled aspects of this problem by calculating the total extraction efficiency for an emitter within a finite size patterned slab. Also relevant is the literature on reflectivity properties of shallow patterned waveguides,[8,9] though many of the methods used are not applicable to the deeply patterned two-dimensional structures considered in this paper.

The aim of the present treatment is to take an arbitrary patterned multilayer structure and calculate reflectivity or transmission spectra for light incident from the outside, or emission spectra from an internal dipole source. The approach adopted is based on the transfer-matrix (*T*-matrix) method, which is widely used to calculate the reflectivity properties of unpatterned multilayer structures.[10] For unpatterned structures, the *T*-matrix is calculated independently for different values of the in-plane wave vector $\mathbf{k}$, by expanding the fields in each layer in terms of plane waves with the corresponding perpendicular wave vector q and applying, electromagnetic boundary conditions at the interfaces. Adding periodic patterning couples $\mathbf{k}$ values, which differ by reciprocal lattice vectors $\mathbf{G}$. Thus, the *T*-matrix, in principle, transfers an infinite set of amplitudes across the structure, giving the Fourier components of the fields at wave vectors $\mathbf{k}+\mathbf{G}$. The field in each layer has to be expanded in terms of the corresponding infinite set of plane waves, obtained by solving the photonic band structure in the layer. Of course, in a real numerical calculation, the set of reciprocal lattice vectors is truncated at large $\mathbf{G}$ values.

In practice, the *T*-matrix is numerically badly behaved in this application: waves with large in-plane $\mathbf{k}+\mathbf{G}$ exhibit strongly evanescent behavior in the perpendicular z direction. The rapidly growing amplitudes that this implies soon lead to numerical overflow. Rather than dealing directly with the *T*-matrix, a better computational approach is to calculate the related scattering matrix (*S*-matrix), introduced by Ko and Inkson.[11] While the *T*-matrix gives the amplitudes of both incoming and outgoing waves at the surface in terms of those in the substrate, the *S*-matrix relates the amplitudes of

the outgoing waves at the surface and in the substrate, to those of the incoming waves on either side of the structure. The original development of the *S*-matrix method, in Ref. 11, was in the context of electron tunneling through multilayer semiconductor structures; the tunneling problem, when the full band structure in individual layers is properly taken into account, has obvious analogies to that of photon transmission through a patterned dielectric structure.

The outline of the remainder of the paper is as follows: In Sec. II, Maxwell's equations are cast in an in-plane momentum representation. Then in Sec. III, the band structure is solved in each layer, ignoring its boundaries, to obtain a set of states that propagate in the z direction as simple plane waves $\exp(iqz)$. In Sec. IV, these are used to form an expansion of the field in terms of forward and backward propagating plane waves. Section V describes how the *S*-matrix is calculated, using this plane wave representation. Sections VI and VII show how the *S*-matrix is used to calculate reflectivity and emission. A brief account of some important numerical considerations is given in Sec. VIII, with particular emphasis on the convergence properties. Finally, in Sec. IX, numerical reflectivity and emission spectra are presented and discussed.

II. MAXWELL'S EQUATIONS

Assuming a harmonic time dependence $\exp(-i\omega t)$ for all fields, Maxwell's equations in a dielectric medium are $\nabla\cdot\varepsilon_0\varepsilon\mathbf{E}=0$, $\nabla\cdot\mathbf{H}=0$, $\nabla\times\mathbf{H}=-i\omega\varepsilon_0\varepsilon\mathbf{E}$, and $\nabla\times\mathbf{E}=i\omega\mu_0\mathbf{H}$. Note that for harmonic fields the first equation is automatically implied by the third. The second can be satisfied by expanding the $\mathbf{H}$ field in basis states with zero divergence. Rescaling $\omega\varepsilon_0\mathbf{E}\rightarrow\mathbf{E}$ and $\sqrt{\mu_0\varepsilon_0}\omega=\omega/c\rightarrow\omega$, the final pair of equations become

$$\nabla\times\mathbf{H}=-i\varepsilon\mathbf{E} \tag{2.1a}$$

$$\nabla\times\mathbf{E}=i\omega^2\mathbf{H}. \tag{2.1b}$$

Within each layer of the structure, ε is independent of z, so it can be written $\varepsilon_l(\mathbf{r})$, where the index l labels the layer. Such l labels will be suppressed in Secs. II to IV, where only a single layer is considered. $\varepsilon(\mathbf{r})$ depends periodically on $\mathbf{r}$, which makes it convenient to work in a momentum representation for the in-plane coordinate, and, for a given Bloch wave vector $\mathbf{k}$, expand the fields as a sum over reciprocal lattice vectors $\mathbf{G}$:

$$\mathbf{H}(\mathbf{r},z)=\sum_{\mathbf{G}}\tilde{\mathbf{H}}_{\mathbf{k}}(\mathbf{G},z)e^{i(\mathbf{k}+\mathbf{G})\cdot\mathbf{r}}. \tag{2.2}$$

For compactness of notation, it is useful to define the Fourier space vector $\boldsymbol{h}(z)=[\tilde{\mathbf{H}}_{\mathbf{k}}(\mathbf{G}_1,z),\tilde{\mathbf{H}}_{\mathbf{k}}(\mathbf{G}_2,z)\ldots]^T$. Note that, although $\tilde{\mathbf{H}}_{\mathbf{k}}(\mathbf{G},z)$ depends on $\mathbf{k}$, the whole calculation is carried out for a fixed value of $\mathbf{k}$, so such labels will be suppressed in other symbols. The momentum representations of $\mathbf{E}$, $\tilde{\mathbf{E}}_{\mathbf{k}}(\mathbf{G},z)$ and $\boldsymbol{e}(z)$, are defined in an equivalent way.

It is also necessary to introduce the Fourier expansion of the dielectric function for the layer,

$$\tilde{\varepsilon}(\mathbf{G})=\frac{1}{S}\int_{\substack{\text{unit}\\\text{cell}}}d\mathbf{r}\,\varepsilon(\mathbf{r})e^{i\mathbf{G}\cdot\mathbf{r}}, \tag{2.3}$$

and the matrix $\hat{\varepsilon}$ such that $\hat{\varepsilon}_{\mathbf{GG}'}=\tilde{\varepsilon}(\mathbf{G}-\mathbf{G}')$. S is the area of the in-plane unit cell. Using equivalent definitions, the reciprocal of the dielectric function $\eta(\mathbf{r})=\varepsilon^{-1}(\mathbf{r})$ has a Fourier expansion $\tilde{\eta}(\mathbf{G})$ and matrix representation $\hat{\eta}$. Note that the matrix product $\hat{\varepsilon}\,\hat{\eta}=1$, provided there is no high-momentum cutoff in the set of reciprocal lattice vectors.

With this Fourier vector notation, the momentum representation of a product such as $\varepsilon\mathbf{E}$ becomes $\hat{\varepsilon}\boldsymbol{e}$. Thus, the final pair of Maxwell's equations, Eqs. (2.1a) and (2.1b), can be written, in component form, as

$$i\hat{k}_y h_z(z)-h_y'(z)=-i\hat{\varepsilon}e_x(z) \tag{2.4a}$$

$$h_x'(z)-i\hat{k}_x h_z(z)=-i\hat{\varepsilon}e_y(z) \tag{2.4b}$$

$$i\hat{k}_x h_y(z)-i\hat{k}_y h_x(z)=-i\hat{\varepsilon}e_z(z) \tag{2.4c}$$

and

$$i\hat{k}_y e_z(z)-e_y'(z)=i\omega^2 h_x(z) \tag{2.5a}$$

$$e_x'(z)-i\hat{k}_x e_z(z)=i\omega^2 h_y(z) \tag{2.5b}$$

$$i\hat{k}_x e_y(z)-i\hat{k}_y e_x(z)=i\omega^2 h_z(z), \tag{2.5c}$$

where $\hat{k}_x,\hat{k}_y$ are diagonal matrices with $(\hat{k}_x)_{\mathbf{GG}}=(k_x+G_x)$ and $(\hat{k}_y)_{\mathbf{GG}}=(k_y+G_y)$, and the primes denote differentiation with respect to z.

The notation introduced in this section to distinguish various types of vector and matrix is adopted in the remainder of the paper: Bold faces denote three vectors ($\mathbf{E}$,$\mathbf{H}$), while lower case italics are used for Fourier space vectors ($\boldsymbol{e}$,$\boldsymbol{h}$). For a finite system with N_G reciprocal lattice vectors, the matrices that occur are mostly of dimension $N_G\times N_G$, indicated by hatted lower case ($\hat{\varepsilon}$, $\hat{\eta}$), or $2N_G\times 2N_G$, for which various upper case symbols will be used ($\mathcal{E}$, $\mathcal{H}$, Φ).

III. SOLVING THE LAYER BAND STRUCTURE

This section is concerned with solving the band structure for an unbounded patterned layer to obtain states which are, in their z dependence, simple plane waves $\exp(iqz)$. The $\mathbf{H}$ field is expanded in basis states with zero divergence, thus guaranteeing $\nabla\cdot\mathbf{H}=0$, and the coefficients in this expansion determined by substituting into Maxwell's equations.

Choosing a symmetric pair of basis states, the z propagating plane wave is expanded as

$$\mathbf{H}(\mathbf{r},z)=\sum_{\mathbf{G}}\left(\phi_x(\mathbf{G})\left[\hat{\mathbf{x}}-\frac{1}{q}(k_x+G_x)\hat{\mathbf{z}}\right]+\phi_y(\mathbf{G})\left[\hat{\mathbf{y}}-\frac{1}{q}(k_y+G_y)\hat{\mathbf{z}}\right]\right)e^{i(\mathbf{k}+\mathbf{G})\cdot\mathbf{r}+iqz}, \tag{3.1}$$

where $\hat{\mathbf{x}}$, $\hat{\mathbf{y}}$, and $\hat{\mathbf{z}}$ are the conventional unit vectors defining the coordinate axes and $\phi_x(\mathbf{G})$, $\phi_y(\mathbf{G})$ are expansion coefficients. It is easily shown that this form satisfies $\nabla\cdot\mathbf{H}=0$.

Translating into the momentum representation, we define vectors $\phi_x=[\phi_x(\mathbf{G}_1),\phi_x(\mathbf{G}_2),\ldots]^T$ and $\phi_y=[\phi_y(\mathbf{G}_1),\phi_y(\mathbf{G}_2),\ldots]^T$, to obtain

$$h(z)=e^{iqz}\left\{\phi_x\hat{\mathbf{x}}+\phi_y\hat{\mathbf{y}}-\frac{1}{q}(\hat{k}_x\phi_x+\hat{k}_y\phi_y)\hat{\mathbf{z}}\right\}, \quad (3.2)$$

where $\hat{k}_x$ and $\hat{k}_y$ are the diagonal matrices defined in Sec. II. Substituting Eq. (3.2) in Eq. (2.4), and multiplying through by $i\hat{\eta}$, gives the momentum representation of **E**:

$$\boldsymbol{e}(z)=\frac{1}{q}\boldsymbol{e}^{iqz}\hat{\eta}\{[\hat{k}_y\hat{k}_x\phi_x+(q^2+\hat{k}_y\hat{k}_y)\phi_y]\hat{\mathbf{x}} -[\hat{k}_x\hat{k}_y\phi_y+(q^2+\hat{k}_x\hat{k}_x)\phi_x]\hat{\mathbf{y}}+q[\hat{k}_y\phi_x-\hat{k}_x\phi_y]\hat{\mathbf{z}}\}. \quad (3.3)$$

Finally, substituting these expressions for $\boldsymbol{e}$ and $\boldsymbol{h}$ into the last Maxwell equation, Eq. (2.5), produces three identities, one for each of $\hat{\mathbf{x}}$, $\hat{\mathbf{y}}$, and $\hat{\mathbf{z}}$. The first two are:

$$\omega^2\phi_x=[\hat{k}_y\hat{\eta}\hat{k}_y+\hat{\eta}(q^2+\hat{k}_x\hat{k}_x)]\phi_x+[\hat{\eta}\hat{k}_x\hat{k}_y-\hat{k}_y\hat{\eta}\hat{k}_x]\phi_y$$

$$\omega^2\phi_y=[\hat{k}_x\hat{\eta}\hat{k}_x+\hat{\eta}(q^2+\hat{k}_y\hat{k}_y)]\phi_y+[\hat{\eta}\hat{k}_y\hat{k}_x-\hat{k}_x\hat{\eta}\hat{k}_y]\phi_x. \quad (3.4)$$

It is straightforward to show that the third identity, obtained from the $\hat{\mathbf{z}}$ component, is linearly dependent on the other two and so is automatically satisfied.

In matrix notation, Eq. (3.4) becomes

$$\left\{\begin{pmatrix}\hat{\eta}&0\\0&\hat{\eta}\end{pmatrix}\left[q^2+\begin{pmatrix}\hat{k}_x\hat{k}_x&\hat{k}_x\hat{k}_y\\\hat{k}_y\hat{k}_x&\hat{k}_y\hat{k}_y\end{pmatrix}\right]+\begin{pmatrix}\hat{k}_y\hat{\eta}\hat{k}_y&-\hat{k}_y\hat{\eta}\hat{k}_x\\-\hat{k}_x\hat{\eta}\hat{k}_y&\hat{k}_x\hat{\eta}\hat{k}_x\end{pmatrix}\right\}\times\begin{pmatrix}\phi_x\\\phi_y\end{pmatrix}=\omega^2\begin{pmatrix}\phi_x\\\phi_y\end{pmatrix}. \quad (3.5)$$

Writing the three 2×2 block matrices which appear in Eq. (3.5) as $\mathcal{H}$, K, and $\mathcal{K}$, and defining a vector $\phi=(\phi_x,\phi_y)^T$, gives the more compact form

$$[\mathcal{H}(q^2+K)+\mathcal{K}]\phi=\omega^2\phi. \quad (3.6)$$

This is the eigenvalue equation for ω.

To obtain an eigenvalue equation for q, Eq. (3.6) needs to be multiplied by the inverse of $\mathcal{H}$. This is the matrix $\mathcal{E}$, with block diagonals $\hat{\varepsilon}$, constructed in the same way as $\mathcal{H}$ is from $\hat{\eta}$. Thus, the q eigenvalue equation is

$$[\mathcal{E}(\omega^2-\mathcal{K})-K]\phi=q^2\phi. \quad (3.7)$$

Equation (3.7) is an asymmetric matrix eigenproblem, which may be complex if ε has an imaginary part. A useful orthogonality property, exploited in Sec. IV, can be obtained by multiplying through by $\omega^2-\mathcal{K}$ and using the fact that, from their definitions, $\mathcal{K}K=0$. Then, Eq. (3.7) becomes

$$[(\omega^2-\mathcal{K})\mathcal{E}(\omega^2-\mathcal{K})-\omega^2K]\phi=q^2(\omega^2-\mathcal{K})\phi, \quad (3.8)$$

which has the form of a generalized symmetric eigenproblem. It follows that the eigenvectors ϕ_n, $\phi_{n'}$ corresponding to eigenvalues q_n, $q_{n'}$ satisfy the orthogonality relationship[12]

$$\phi_n^T(\omega^2-\mathcal{K})\phi_{n'}=\delta_{nn'}. \quad (3.9)$$

Note that as the matrix $\omega^2-\mathcal{K}$ is not positive definite, it is no easier to solve the generalized symmetric problem than the asymmetric problem. It also means that complex q^2 eigenvalues can occur even for real ε.

IV. ELECTRIC AND MAGNETIC FIELDS

The next stage of the solution consists of using the propagating wave eigenstates defined in Sec. III as basis states to construct the fields in each layer of the structure. The fields can be expressed as a combination of forward and backward propagating waves with wave numbers q_n, and complex amplitudes a_n and b_n, respectively. These amplitudes are to be determined by applying the boundary conditions at the interfaces and surfaces of the structure. This section shows how to go between a description of the field in terms of amplitudes to one in terms of the field components e_x, e_y, h_x, and h_y. This is a necessary part of the solution, as the electromagnetic boundary conditions at the interfaces are expressed in terms of the continuity of these in-plane field components.

From the momentum representation of **H** defined in Eq. (3.2), the in-plane components of $\boldsymbol{h}$ are expanded in terms of the propagating waves as

$$\begin{pmatrix}h_x(z)\\h_y(z)\end{pmatrix}=\sum_n\begin{pmatrix}\phi_{x_n}\\\phi_{y_n}\end{pmatrix}(e^{iq_nz}a_n+e^{iq_n(d-z)}b_n), \quad (4.1)$$

where d is the thickness of the layer. Note that a_n is the coefficient of the forward going wave at the $z=0$ interface, and b_n that of the backward going wave at $z=d$. Thus, if the arbitrary sign in q_n is chosen to make $\mathrm{Im}\{q_n\}>0$, the defined coefficient is the maximum amplitude of each wave in the layer.

Looking again for a more compact notation, we define a matrix Φ whose columns are the vectors ϕ_n, a diagonal matrix $\hat{\mathrm{f}}(z)$, such that $\hat{\mathrm{f}}(z)_{nn}=e^{iq_nz}$, and vectors $h_\parallel(z)=[h_x(z),h_y(z)]^T$, $a=(a_1,a_2\ldots)^T$ and $b=(b_1,b_2\ldots)^T$. In terms of these quantities, the in-plane magnetic-field components become

$$h_\parallel(z)=\Phi[\hat{\mathrm{f}}(z)a+\hat{\mathrm{f}}(d-z)b]. \quad (4.2)$$

Similarly, using the momentum representation of **E** from Eq. (3.3), the in-plane components of the electric field are

$$\begin{pmatrix}-e_y(z)\\e_x(z)\end{pmatrix}=\sum_n\begin{pmatrix}\hat{\eta}&0\\0&\hat{\eta}\end{pmatrix}\left[q_n^2+\begin{pmatrix}\hat{k}_x\hat{k}_x&\hat{k}_x\hat{k}_y\\\hat{k}_y\hat{k}_x&\hat{k}_y\hat{k}_y\end{pmatrix}\right]\times\begin{pmatrix}\phi_{x_n}\\\phi_{y_n}\end{pmatrix}\frac{1}{q_n}(e^{iq_nz}a_n-e^{iq_n(d-z)}b_n). \quad (4.3)$$

Identifying the block matrices $\mathcal{H}$ and K of Sec. III, and defining $e_\parallel(z)=[-e_y(z),e_x(z)]^T$ (note the skew), this becomes

$$e_\parallel(z)=\sum_n\mathcal{H}(K+q_n^2)\phi_n\frac{1}{q_n}(e^{iq_nz}a_n-e^{iq_n(d-z)}b_n). \quad (4.4)$$

Equation (4.4) can be put in the same notation as Eq. (4.2) by defining a diagonal matrix $\hat{q}$ such that $\hat{q}_{nn}=q_n$, and using the eigenvalue equation for ω, Eq. (3.6), to replace $\mathcal{H}(K+q_n^2)\phi_n$ by $(\omega^2-\mathcal{K})\phi_n$

$$e_{\|}(z)=(\omega^2-\mathcal{K})\Phi\hat{q}^{-1}[\hat{\mathrm{f}}(z)a-\hat{\mathrm{f}}(d-z)b]. \tag{4.5}$$

Equations (4.2) and (4.5) combined give

$$\begin{pmatrix} e_{\|}(z) \\ h_{\|}(z) \end{pmatrix}=\begin{pmatrix} (\omega^2-\mathcal{K})\Phi\hat{q}^{-1} & -(\omega^2-\mathcal{K})\Phi\hat{q}^{-1} \\ \Phi & \Phi \end{pmatrix}\begin{pmatrix} \hat{\mathrm{f}}(z)a \\ \hat{\mathrm{f}}(d-z)b \end{pmatrix}$$
$$=M\begin{pmatrix} \hat{\mathrm{f}}(z)a \\ \hat{\mathrm{f}}(d-z)b \end{pmatrix}. \tag{4.6}$$

Using the orthogonality relationship Eq. (3.9), which in matrix form is $\Phi^T(\omega^2-\mathcal{K})\Phi=1$, it is easily verified that the inverse of M is

$$M^{-1}=\tfrac{1}{2}\begin{pmatrix} \hat{q}\Phi^T & \Phi^T(\omega^2-\mathcal{K}) \\ -\hat{q}\Phi^T & \Phi^T(\omega^2-\mathcal{K}) \end{pmatrix}. \tag{4.7}$$

V. THE SCATTERING MATRIX

This section describes how the S-matrix for the structure is constructed from the solutions to the q eigenvalue problem. The solutions for the different layers are combined, so l labels need to be added to the various matrices and vectors defined for the individual layers.

The S-matrix relates the vectors of the amplitudes of forward and backward going waves, a_l and b_l, in different layers of the structure:

$$\begin{pmatrix} a_l \\ b_{l'} \end{pmatrix}=S(l',l)\begin{pmatrix} a_{l'} \\ b_l \end{pmatrix}=\begin{pmatrix} S_{11} & S_{12} \\ S_{21} & S_{22} \end{pmatrix}\begin{pmatrix} a_{l'} \\ b_l \end{pmatrix}. \tag{5.1}$$

Note again that the definition is skewed: the S-matrix relates a_l and $b_{l'}$ to $a_{l'}$ and b_l. This is in contrast to the T-matrix, which relates pairs of waves in the same layers. It is this difference which makes the S-matrix numerically more stable than the T-matrix when evanescent waves are involved.

The amplitudes in each layer are related by the interface matrix $I(l,l+1)$ defined by

$$\begin{pmatrix} \hat{f}_l a_l \\ b_l \end{pmatrix}=I(l,l+1)\begin{pmatrix} a_{l+1} \\ \hat{f}_{l+1}b_{l+1} \end{pmatrix}=\begin{pmatrix} I_{11} & I_{12} \\ I_{21} & I_{22} \end{pmatrix}\begin{pmatrix} a_{l+1} \\ \hat{f}_{l+1}b_{l+1} \end{pmatrix}, \tag{5.2}$$

where $\hat{f}_l=\hat{\mathrm{f}}_l(d_l)$. The interface matrix is obtained by requiring that the fields on either side of the interface satisfy the electromagnetic boundary conditions, that is continuity of the in-plane components E_x, E_y, H_x, H_y, and thus the vectors $e_{\|}$ and $h_{\|}$. Using Eq. (4.6) with $z=d_l$ in layer l, and $z=0$ in layer $l+1$, these boundary conditions give

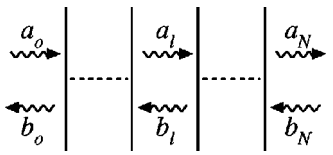

FIG. 1. Labeling scheme for forward and backward going waves in different layers of the structure. $l=0$ is the surface, $l=N$ the substrate.

$$I(l,l+1)=M_l^{-1}M_{l+1}$$
$$=\tfrac{1}{2}\hat{q}_l\Phi_l^T(\omega^2-\mathcal{K}_{l+1})\Phi_{l+1}\hat{q}_{l+1}^{-1}\begin{pmatrix} 1 & -1 \\ -1 & 1 \end{pmatrix}$$
$$+\tfrac{1}{2}\Phi_l^T(\omega^2-\mathcal{K}_l)\Phi_{l+1}\begin{pmatrix} 1 & 1 \\ 1 & 1 \end{pmatrix}. \tag{5.3}$$

The S-matrix is built up a layer at a time, with $S(l',l+1)$ calculated from $S(l',l)$ using the definition of $S(l',l)$ in Eq. (5.1) and the interface matrix $I(l,l+1)$. Eliminating a_l and b_l gives relationships between $a_{l'}$, $b_{l'}$ and a_{l+1}, b_{l+1}, from which $S(l',l+1)$ can be constructed. This leads to the following recipe:

$$S_{11}(l',l+1)=(I_{11}-\hat{f}_l S_{12}(l',l)I_{21})^{-1}\hat{f}_l S_{11}(l',l)$$

$$S_{12}(l',l+1)=(I_{11}-\hat{f}_l S_{12}(l',l)I_{21})^{-1}$$
$$\times(\hat{f}_l S_{12}(l',l)I_{22}-I_{12})\hat{f}_{l+1}$$

$$S_{21}(l',l+1)=S_{22}(l',l)I_{21}S_{11}(l',l+1)+S_{21}(l',l)$$

$$S_{22}(l',l+1)=S_{22}(l',l)I_{21}S_{12}(l',l+1)+S_{22}(l',l)I_{22}\hat{f}_{l+1}. \tag{5.4}$$

Starting from $S(l',l')=1$, Eq. (5.4) is applied a layer at a time to build up $S(l',l)$. The mathematical reason for the stability of the S-matrix is apparent from Eq. (5.4): with $\mathrm{Im}\{q_n\}>0$, all the elements of $\hat{f}$ have absolute value less than unity, and since $\hat{f}$ is never inverted directly, the evanescent waves do not cause the exponential growth which gives problems in a transfer-matrix calculation. This argument is not affected by the matrix inversion in the first two equations, which is dominated by the nonsingular I_{11}.

Labeling the surface $l=0$ and the substrate $l=N$ (see Fig. 1), reflectivity and transmission coefficients are obtained from $S(0,N)$. The details of this procedure are explained in Sec. VI. Emission calculations require the two S matrices coupling the source location to the surface and substrate, as described in Sec. VII. It can also be useful to be able to calculate the fields within the structure, which requires a knowledge of a_l and b_l. These are obtained by calculating $S(0,l)$ and $S(l,N)$, and using Eq. (5.1) to get

$$a_l=[1-S_{12}(0,l)S_{21}(l,N)]^{-1}$$
$$\times[S_{11}(0,l)a_0+S_{12}(0,l)S_{22}(l,N)b_N]$$

$$b_l=[1-S_{21}(l,N)S_{12}(0,l)]^{-1}$$
$$\times[S_{21}(l,N)S_{11}(0,l)a_0+S_{22}(l,N)b_N]. \tag{5.5}$$

VI. REFLECTIVITY

Once the *S*-matrix has been calculated according to Sec. V, reflectivity, and transmission, spectra are easily obtained. For an experiment in which light is incident on the surface, a_0 is determined by the incident geometry and $b_N=0$. Then, the reflected wave has amplitude $b_0=S_{21}(0,N)a_0$, and the transmitted wave in the substrate $a_N=S_{11}(0,N)a_0$. It is thus only necessary to translate the amplitudes a_0, b_0, and a_N into experimental angle and polarization-dependent external plane waves. This is best done by using Eq. (4.6) to pass between amplitude and electromagnetic-field representations, and expressing the external plane waves in terms of these fields.

An external plane wave is specified by its polarization and direction of propagation, defined by polar coordinates (θ,ϕ) relative to the surface normal (see Fig. 3). Writing $k_0=\sqrt{\varepsilon}\omega/c$, where ε is the dielectric constant of the external medium, the in-plane wave vector is

$$\mathbf{k}=k_0\sin\theta(\cos\phi\hat{\mathbf{x}}+\sin\phi\hat{\mathbf{y}}). \tag{6.1}$$

Then TE- and TM-polarized plane waves are given by field components

$$\mathbf{E}_{\mathrm{TE}}=\varepsilon_0\omega c Z^{1/2}(\sin\phi\hat{\mathbf{x}}-\cos\phi\hat{\mathbf{y}})e^{i(\mathbf{k}\cdot\mathbf{r}+qz)}$$

$$\mathbf{H}_{\mathrm{TE}}=Z^{-1/2}(\cos\theta\cos\phi\hat{\mathbf{x}}+\cos\theta\sin\phi\hat{\mathbf{y}}-\sin\theta\hat{\mathbf{z}})e^{i(\mathbf{k}\cdot\mathbf{r}+qz)}$$

$$\mathbf{E}_{\mathrm{TM}}=\varepsilon_0\omega c Z^{1/2}(\cos\theta\cos\phi\hat{\mathbf{x}}+\cos\theta\sin\phi\hat{\mathbf{y}}-\sin\theta\hat{\mathbf{z}})\times e^{i(\mathbf{k}\cdot\mathbf{r}+qz)}$$

$$\mathbf{H}_{\mathrm{TM}}=Z^{-1/2}(-\sin\phi\hat{\mathbf{x}}+\cos\phi\hat{\mathbf{y}})e^{i(\mathbf{k}\cdot\mathbf{r}+qz)}, \tag{6.2}$$

where $Z=\sqrt{\mu_0/(\varepsilon_0\varepsilon)}$ is the intrinsic impedance of the external medium. Note that the **E** fields here are scaled (see Sec. II): the normalization is chosen so that the true Poynting vector, $(\varepsilon_0\omega c)^{-1}\mathbf{E}\times\mathbf{H}$, has unit magnitude.

Consider first a lattice with a period sufficiently short that all the scattering states (for which $k<k_0$) on either side of the structure lie within the first Brillouin zone. For the incident wave, the $\mathbf{G}=0$ components of the $\boldsymbol{e}$ and $\boldsymbol{h}$ fields are then given by Eq. (6.2), and all $\mathbf{G}\neq 0$ components are zero. Thus, the incident amplitude a_0 is obtained directly from Eqs. (6.2) and (4.6). The reflected and transmitted waves are found by taking the $\mathbf{G}=0$ components of the fields which correspond to the calculated b_0 and a_N and resolving them into TE and TM contributions using Eq. (6.2). In this case, the $\mathbf{G}\neq 0$ components are all evanescent waves outside the structure, and so do not contribute to the far field.

The situation is more complicated when the lattice period is large enough to give scattering states outside the first Brillouin zone, so that diffraction can occur. Then, conventionally, **k** is brought into the first zone by subtracting the appropriate reciprocal lattice vector **G**, and the incident $\boldsymbol{e}$ and $\boldsymbol{h}$ fields have only the corresponding finite **G** component. The reflected and transmitted fields generally have a number of finite **G** components, which are propagating waves, and so lead to diffracted features in the far field. The directions in which diffraction occurs are found by adding these **G** values to **k** and inverting Eq. (6.1) to obtain θ and ϕ.

VII. EMISSION

This section addresses the problem of calculating the emission from an oscillating point dipole placed inside the structure. The boundary conditions in an emission problem are different from reflectivity and transmission: there is no incoming wave, but instead an additional internal condition, that of a field discontinuity at the position of the dipole. This internal boundary condition is first derived, and then incorporated into the *S*-matrix formalism to obtain the external emission.

The source to be treated is an oscillating point dipole, with harmonic time dependence, at position $(\mathbf{r}_0,z_0)$. In this paper, we consider only the weak coupling limit, so the amplitude of the dipole $\mathbf{J}_0$ is independent of the the local fields. The spatial dependence of the current density **J** is

$$\mathbf{J}(\mathbf{r},z)=\mathbf{J}_0\delta(\mathbf{r}-\mathbf{r}_0)\,\delta(z-z_0)=\sum_{\mathbf{k},\mathbf{G}}\tilde{\mathbf{J}}_{\mathbf{k}}(\mathbf{G})e^{i(\mathbf{k}+\mathbf{G})\cdot\mathbf{r}}\delta(z-z_0), \tag{7.1}$$

where $\tilde{\mathbf{J}}_{\mathbf{k}}(\mathbf{G})=\mathbf{J}_0e^{-i(\mathbf{k}+\mathbf{G})\cdot\mathbf{r}_0}$. Although the expansion in Eq. (7.1) contains all values of **k**, $\tilde{\mathbf{J}}_{\mathbf{k}}(\mathbf{G})$ fully determines the emission into modes with wave vector **k**. Hence, the calculation can be performed independently for each value of **k**, and again **k** labels will be suppressed.

With a source term added, Maxwell's equations are modified, so Eq. (2.1a) becomes $\boldsymbol{\nabla}\times\mathbf{H}=\mathbf{J}-i\varepsilon\mathbf{E}$. Defining the vector $\boldsymbol{j}=[\tilde{\mathbf{J}}_{\mathbf{k}}(\mathbf{G}_1),\tilde{\mathbf{J}}_{\mathbf{k}}(\mathbf{G}_2)\ldots]^T$, in the momentum representation this is written

$$i\hat{k}_yh_z(z)-h_y'(z)=j_x\delta(z-z_0)-i\hat{\varepsilon}e_x(z) \tag{7.2a}$$

$$h_x'(z)-i\hat{k}_xh_z(z)=j_y\delta(z-z_0)-i\hat{\varepsilon}e_y(z) \tag{7.2b}$$

$$i\hat{k}_xh_y(z)-i\hat{k}_yh_x(z)=j_z\delta(z-z_0)-i\hat{\varepsilon}e_z(z). \tag{7.2c}$$

The in-plane and perpendicular components of **J** are best treated separately. Consider first the in-plane component, putting $j_z=0$. In order to cancel the singular term due to the source in Eqs. (7.2a) and (7.2b), there must be discontinuities in h_y and h_x at $z=z_0$ of $-j_x$ and j_y respectively. h_z, e_x, and e_y are all continuous, but there is a discontinuity in e_z by Eq. (7.2c), of $\hat{\eta}(\hat{k}_xj_x+\hat{k}_yj_y)$. It is easily shown that with these discontinuities, and obtaining the charge density ρ using $\boldsymbol{\nabla}\cdot\mathbf{J}=i\omega\rho$, all of Maxwell's equations are satisfied. Thus, writing $p_\parallel=(j_y,-j_x)^T$, the required boundary conditions on the in-plane components of the fields are

$$e_\parallel(z_0^+)-e_\parallel(z_0^-)=0$$

$$h_\parallel(z_0^+)-h_\parallel(z_0^-)=p_\parallel. \tag{7.3}$$

Turning to the perpendicular component of **J**, put $j_x=j_y=0$. Then the singular term in Eq. (7.2c) is cancelled by a similar singularity in e_z, that is $e_z(z)=-i\hat{\eta}j_z\delta(z-z_0)+$ nonsingular parts. This introduces singular terms into the left-hand side of the Maxwell Eqs. (2.5a) and (2.5b), which are cancelled by discontinuities in e_x and e_y of $\hat{k}_x\hat{\eta}j_z$ and $\hat{k}\hat{\eta}j_z$ respectively.[13] Again, these are the only discontinuities: h_x, h_y, and h_z are all continuous. Defining p_z

$=(-\hat{k}_y\hat{\eta}j_z,\hat{k}_x\hat{\eta}j_z)^T$, the boundary conditions on the in-plane components of the fields are thus

$$e_\parallel(z_0^+)-e_\parallel(z_0^-)=p_z$$

$$h_\parallel(z_0^+)-h_\parallel(z_0^-)=0. \tag{7.4}$$

The discontinuity condition can now be combined with the *S*-matrix treatment to calculate the emission from the structure. Consider an arbitrarily oriented dipole placed at the interface between layers l and $l+1$, so the boundary conditions become

$$\begin{pmatrix} e_{\parallel_{l+1}}(0) \\ h_{\parallel_{l+1}}(0) \end{pmatrix} - \begin{pmatrix} e_{\parallel_l}(d_l) \\ h_{\parallel_l}(d_l) \end{pmatrix} = \begin{pmatrix} p_z \\ p_\parallel \end{pmatrix}. \tag{7.5}$$

Using Eq. (4.6) this condition is expressed in terms of the propagating wave amplitudes as

$$M_{l+1}\begin{pmatrix} a_{l+1} \\ \hat{f}_{l+1}b_{l+1} \end{pmatrix} - M_l\begin{pmatrix} \hat{f}_l a_l \\ b_l \end{pmatrix} = \begin{pmatrix} p_z \\ p_\parallel \end{pmatrix}. \tag{7.6}$$

The external boundary condition for an emission problem is that there should be only outgoing waves, that is $a_0=b_N=0$. Taking the definitions of the *S*-matrices $S(0,l)$ and $S(l+1,N)$ from Eq. (5.1), it follows that

$$a_l = S_{12}(0,l)b_l \tag{7.7a}$$

$$b_0 = S_{22}(0,l)b_l \tag{7.7b}$$

$$a_N = S_{11}(l+1,N)a_{l+1} \tag{7.7c}$$

$$b_{l+1} = S_{21}(l+1,N)a_{l+1}. \tag{7.7d}$$

Substituting for a_l and b_{l+1} from Eqs. (7.7a) and (7.7d) in Eq. (7.6):

$$M_{l+1}\begin{pmatrix} a_{l+1} \\ \hat{f}_{l+1}S_{21}(l+1,N)a_{l+1} \end{pmatrix} - M_l\begin{pmatrix} \hat{f}_l S_{12}(0,l)b_l \\ b_l \end{pmatrix} = \begin{pmatrix} p_z \\ p_\parallel \end{pmatrix}. \tag{7.8}$$

Finally, putting in the explicit form for M_l, M_{l+1}, expanding and rearranging, gives

$$\begin{pmatrix} (\omega^2-\mathcal{K}_{l+1})\Phi_{l+1}\hat{q}_{l+1}^{-1}[1-\hat{f}_{l+1}S_{21}(l+1,N)] & (\omega^2-\mathcal{K}_l)\Phi_l\hat{q}_l^{-1}[1-\hat{f}_l S_{12}(0,l)] \\ \Phi_{l+1}[1+\hat{f}_{l+1}S_{21}(l+1,N)] & -\Phi_l[1+\hat{f}_l S_{12}(0,l)] \end{pmatrix}\begin{pmatrix} a_{l+1} \\ b_l \end{pmatrix} = \begin{pmatrix} p_z \\ p_\parallel \end{pmatrix}. \tag{7.9}$$

The emission is thus calculated by solving Eq. (7.9) for a_{l+1} and b_l, and using Eqs. (7.7b) and (7.7c) to obtain b_0 and a_N, the outgoing waves at the surface and in the substrate. These are then translated into TE and TM intensities using Eqs. (6.2) and (4.6), as in the reflectivity calculations of Sec. VI.

VIII. NUMERICAL METHODS AND CONVERGENCE

Most of the numerical work in the treatment developed in the preceding sections can be carried out using standard routines available in most linear algebra packages.[14] The routines required are a nonsymmetric matrix solver to obtain eigenvalues and eigenvectors for the layer band structure from Eq. (3.7), a complex matrix inverter for constructing the *S*-matrix using Eq. (5.4), and a complex simultaneous equation solver for Eq. (7.9) in the emission problem. The matrix eigenvalue solver has to cope with complex matrices if there is absorption in the structure and the refractive indices are not entirely real. For nondegenerate q eigenvalues, the orthogonality condition Eq. (3.9) is a property of the eigenvectors, so is automatically satisfied. However, the usual normalization has to be corrected to include the matrix $\omega^2-\mathcal{K}$. Similarly, for degenerate sets of eigenvalues, standard linear algebra routines typically, but arbitrarily, produce mutually orthogonal eigenvectors. In order to satisfy Eq. (3.9) these have to be re-orthogonalized. The method adopted here is a generalized version of the modified Gram-Schmidt process,[15] in which $\omega^2-\mathcal{K}$ is inserted into all inner products. For unpatterned layers, where the eigenvalues always come in degenerate pairs, it is better to generate states with the correct orthogonality property ''by hand.''

The calculated fields are only exact solutions to Maxwell's equations in the limit where a complete, infinite set of reciprocal lattice vectors is used. In a real calculation, there are inaccuracies when this is truncated to a finite set of N_G vectors by applying a high-momentum cutoff. One effect of this cutoff is that the matrices $\hat{\varepsilon}$ and $\hat{\eta}$, defined in Sec. II, are no longer mutual inverses. There are various ways in which this can be handled: $\hat{\varepsilon}$ and $\hat{\eta}$ can be calculated according to their definitions, in which case $\hat{\varepsilon}\hat{\eta}\neq 1$, or one or other matrix can be calculated directly, and the other obtained by matrix inversion. For band-structure calculations, it is known[16] that the best convergence is obtained when $\hat{\varepsilon}$ is calculated directly and inverted to obtain $\hat{\eta}$. The same rule seems to apply to the present calculations, and indeed for lattices with simple unit cells, very rapid convergence is obtained in this way. The convergence is illustrated in Fig. 2, where spectra are plotted with increasing N_G for the same set of physical parameters. Though the $N_G=9$ spectrum differs qualitatively from the rest, for $N_G=25$ and higher only small quantitative changes occur. The differences in energy of the sharp features for $N_G=121$ and $N_G=169$ are, at most, $\sim$0.5 meV. If, on the other hand, $\hat{\eta}$ is calculated directly and $\hat{\varepsilon}$ obtained by inversion (not shown), even for $N_G=169$ the spectra are still a long way from convergence.

The $N_G=121$ calculations are very practical, taking only about 30 s for each point on the spectrum (for a structure consisting of four layers, two of which are patterned) using an average work station. The nature of the calculation means that this time increases only linearly with the number of layers. However, the time taken for the main matrix opera-

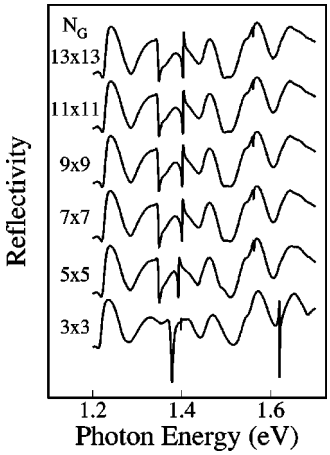

FIG. 2. Calculated reflectivity spectra, showing convergence as the number of reciprocal lattice vectors, N_G, is increased. The spectra are for TE-polarized $\Gamma-K$ reflectivity at $\theta=60°$, as plotted in Fig. 4.

tions scales as $\sim N_G^3$, so problems with complicated lattices, such as supercell defect calculations, would be much more demanding.

IX. NUMERICAL RESULTS

The waveguide structure we have used for the calculations in this paper is shown schematically in Fig. 3. It consists of a 400-nm $Al_{0.12}Ga_{0.88}As$ guide layer, on top of a 1100-nm $Al_{0.35}Ga_{0.65}As$ cladding layer. The substrate is GaAs. The waveguide is patterned with a triangular lattice of circular holes of radius 95 nm and depth 1000 nm. The lattice constant is 360 nm. This structure is similar to the one used in the experiments of Ref. 2. The main difference between that paper and the present calculations is that here we have not included the oxide skin round the holes, which is required to obtain good agreement with experiment. The energy dependent $Al_xGa_{1-x}As$ dielectric constant used in the calculations comes from an approximate formula due to Boyd.[17]

With circular holes, the Fourier expansion of the dielectric function, Eq. (2.3), is easily obtained analytically.[18] For

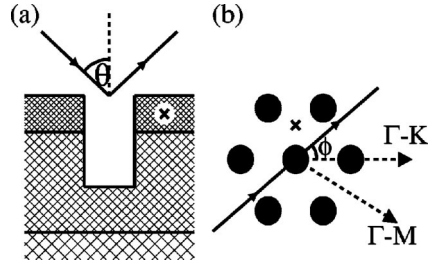

FIG. 3. Schematic views of the structure used in numerical calculations: (a) Cross section, showing a hole passing through the waveguide core into the cladding. (b) Plan view, showing the lattice of holes and examples of the high-symmetry $\Gamma-K$ and $\Gamma-M$ directions. The $\times$ indicates the position of the source in the emission calculations.

holes of radius ρ and dielectric constant $\varepsilon=\varepsilon_a$ in a material with $\varepsilon=\varepsilon_b$,

$$\varepsilon(\mathbf{G})=\begin{cases}2(\varepsilon_a-\varepsilon_b)\beta J_1(G\rho)/(G\rho) & \mathbf{G}\neq 0\\ \varepsilon_a\beta+\varepsilon_b(1-\beta) & \mathbf{G}=0,\end{cases} \tag{9.1}$$

where β is the fraction of the area taken up by holes, and J_1 is a Bessel function. For a triangular lattice, with lattice constant L, $\beta=\frac{2}{3}\sqrt{3}\pi\rho^2/L^2$.

Figure 4 shows reflectivity spectra calculated for TE and TM polarized incident light. The $\Gamma-K$ lattice direction is chosen, and spectra plotted for angles of incidence ranging from 0.1° to 60°. The reflectivity spectra consist of a smooth background variation, upon which sharp resonance features are apparent. These resonances occur at energies for which the external light couples to scattering modes in the waveguide. Just as for shallow gratings,[9] the resonance features can take the form of maxima, minima, or inflections in the reflectivity spectra. Also like shallow gratings, there is no coupling to the waveguide modes at normal incidence, but for a small offset from normal ($\theta=0.1°$), extremely sharp resonance features emerge. As the angle of incidence increases, this feature shifts in energy and broadens, and more resonances appear. Due to the relationship between the incidence geometry and the wave vector k, expressed in Eq. (6.1), the energy variation of the resonances in such angular dependent reflectivity spectra can be used to plot out the

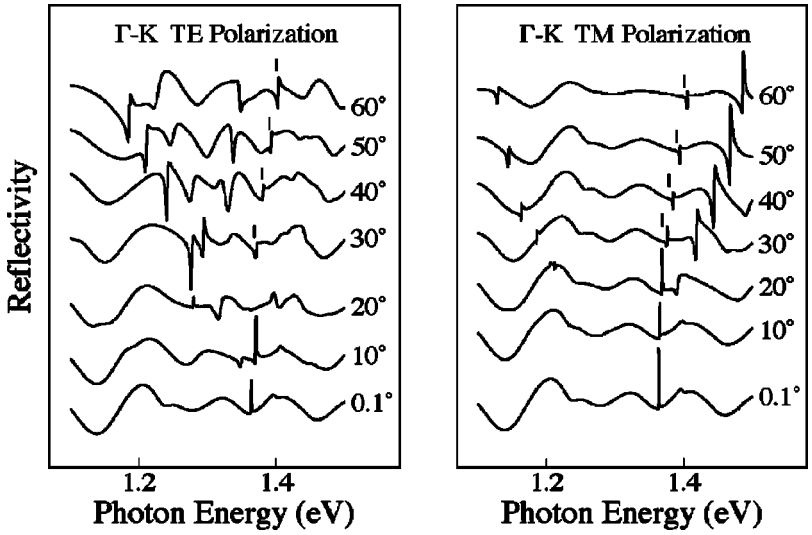

FIG. 4. Calculated reflectivity spectra for various angles of incidence, with TE- and TM-polarized light in the $\Gamma-K$ lattice direction (see Fig. 3). 121 reciprocal lattice vectors were used in the calculations. The marked features in the higher angle spectra correspond to a waveguide mode which is visible in both polarizations.

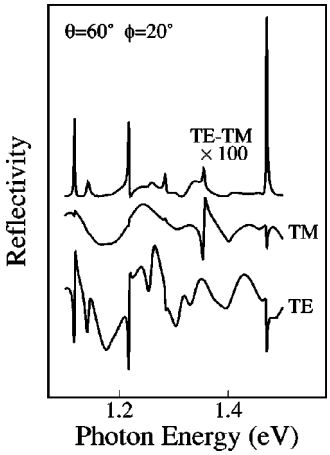

FIG. 5. Calculated reflectivity spectra for $\theta=60°$ in the low-symmetry $\phi=20°$ direction. Three types of reflection are shown: the usual measurements where both incident and reflected light are polarized the same way (TE and TM on the figure), and the much weaker conversion process where the polarizations are orthogonal (TE-TM).

photonic band structure of the waveguide. It was shown in Ref. 2 that the band structure obtained in this way has similarities to the ideal two-dimensional case, but is significantly modified by the waveguide. Unlike the case for shallow gratings, the deeply etched holes in the present structures lead to very significant changes in the band structure, including the formation of large band gaps at the critical points in the Brillouin zone.

As well as revealing the waveguide band structure, the resonances in reflectivity spectra provide information about the strength of the external coupling of the scattering modes for each polarization. Clearly, the most significant features in the spectra must correspond to the modes that couple most strongly. In a structure without absorption, the only damping of the modes is due to this coupling, so the homogeneous linewidth of the resonance features also gives a measure of the total loss rate. This includes both polarizations, and scattering into the substrate as well as through the surface, so the relationship between the strength and linewidths is not simple. Generally, however, the stronger features are indeed broader. It is also interesting to compare the polarization in which a resonance feature appears with that of the underlying mode: it was show in Ref. 2 that, due to the polarization-mixing effects of the patterned waveguide, a predominantly TE-polarized mode can show up in TM-polarized spectra, and vice versa. Occasionally, a single mode appears in both TE and TM spectra, for example, the marked feature in Fig. 4. For the $\Gamma-K$ and $\Gamma-M$ directions, which are lines of reflection symmetry for the lattice, polarization conversion is forbidden: TE incident light cannot be reflected as TM, because a change of parity is involved. However, in lower symmetry directions, where parity is not definable, weak polarization conversion can occur. A typical example is shown in Fig. 5, for the $\phi=20°$ direction. The conversion spectrum, labeled ''TE-TM'' on the figure, is sharply peaked at the energies of the ordinary reflectivity resonances. Understandably, the stronger features correspond to those modes that appear in both TE and TM spectra, but even the largest peak only represents a conversion efficiency of $\sim 0.2\%$.

Angle-dependent emission spectra for our structure are shown in Fig. 6. The source is a dipole oriented in the z direction, perpendicular to the plane of the layers. Its in-plane position is the midpoint of one of the triangles which form the lattice, and it is located at a depth of 200 nm, halfway through the waveguide layer (see Fig. 3). Note that with the symmetry reduced by the addition of the source, the $\Gamma-K$ directions are no longer equivalent: the present calculation corresponds to light emitted in the direction of one of the edges of the triangle containing the source. The tops of the stronger features are truncated in the figure; without such a cutoff, one or two peaks would dominate the spectra, making it difficult to see the detailed structure. We have assumed a ''white'' source, in that without the waveguide the emission would be independent of frequency. This implies that the amplitude of the dipole motion varies as ω^{-2}, and that of the current density, $\mathbf{J}_0$, as ω^{-4}.

The emission features in Fig. 6 follow closely the resonances in the reflectivity spectra of Fig. 4, and are clearly related. Emission can be thought of as a two stage process: the source excites the waveguide modes, and these then scatter out of the guide according to the strength of the coupling

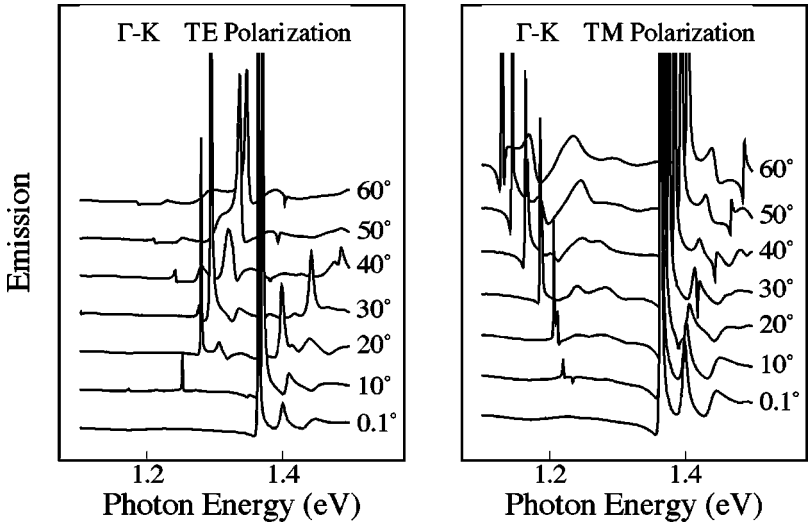

FIG. 6. Calculated emission spectra for the same conditions as Fig. 4. The source is a dipole oriented in the z dir ection. It is located in the center of the waveguide at the midpoint of one of the lattice triangles (see Fig. 3). The strong, sharp peaks are truncated in order to reveal the weaker features in the spectra.

to the external fields. Thus, significant emission only occurs at the energies of the reflectivity resonances, where there is strong external coupling. The actual strength of the emission features is determined by both the external coupling, and the coupling between the source and the waveguide modes. This explains how a perpendicularly oriented dipole can generate TE-polarized emission, which would be impossible without the patterning—the source excites mixed-polarization waveguide modes, which then scatter out to produce external TE-polarized light.

The source coupling depends on the magnitude of the waveguide fields at the location of the dipole. Hence, comparisons of the relative strengths of the emission peaks for different source positions can, in principle, help to map out the spatial variation of the fields. To be more precise, for the perpendicular oriented dipole considered here, the near field **E** in the plane of the source is in the *z* direction, so the source can only excite waveguide modes for which $e_z \neq 0$. As an example, for the source position considered above, which is on a high symmetry line parallel to $\Gamma - M$, no TE polarized light is emitted in the corresponding $\Gamma - M$ direction: parity requires a TE active mode propagating in this direction to have $e_z = 0$ along such a line. Similar considerations apply for in-plane dipoles, though the detailed rules for the coupling of the source to the waveguide mode are obviously different.

X. CONCLUSIONS

We have developed a scattering-matrix treatment that enables us to calculate the electromagnetic properties of multilayer dielectric structures with an arbitrary in-plane periodic patterning. The treatment includes the coupling of the internal electromagnetic modes to external fields, so it provides a straightforward way of calculating reflectivity and emission spectra for patterned waveguide structures.

The computational procedure is numerically stable, and we have shown that it converges rapidly when the dielectric matrices $\hat{\varepsilon}$ and $\hat{\eta}$ are determined in the appropriate way. For simple lattices, the calculation is fast enough to allow accurate spectra to be obtained using a work station or PC.

The reflectivity spectra that we have presented, here and in Ref. 2, have been shown to agree well with experimental results. They provide information about the waveguide photonic band structure, and the external coupling of the guided modes. We have also calculated spectra for light emitted by a dipole source within the structure, and discussed the factors that determine its intensity. An obvious development of these calculations would be to integrate the emitted intensity over the entire Brillouin zone, providing a theoretical determination of the control of the emission rate obtainable in real structures.

[1] T. F. Krauss, R. M. De La Rue, and S. Brand, Nature (London) **383**, 699 (1996).

[2] V. N. Astratov, D. M. Whittaker, I. S. Culshaw, R. M. Stevenson, M. S. Skolnick, T. F. Krauss, and R. M. De La Rue (unpublished).

[3] M. Plihal and A. A. Maradudin, Phys. Rev. B **44**, 8565 (1991); R. D. Meade, K. D. Brommer, A. M. Rappe, and J. D. Joannopulos, Appl. Phys. Lett. **61**, 495 (1992).

[4] K. Sakoda, Phys. Rev. B **52**, 8992 (1995).

[5] D. M. Atkin, P. St. J. Russell, T. A. Birks, and P. J. Roberts, J. Mod. Opt. **41**, 1035 (1996).

[6] M. D. B. Charlton, S. W. Roberts, and G. J. Parker, Mater. Sci. Eng., B **49**, 155 (1997).

[7] S. Fan, P. R. Villeneuve, J. D. Joannopoulos, and E. F. Schubert, Phys. Rev. Lett. **78**, 3294 (1997).

[8] S. L. Chuang and J. A. Kong, J. Opt. Soc. Am. **73**, 669 (1983).

[9] See D. Rosenblatt, A. Sharon, and A. A. Friesem, IEEE J. Quantum Electron. **33**, 2038 (1997), for more recent work and references.

[10] See, for example, E. Hecht, *Optics*, 2nd ed. (Addison Wesley, Reading, MA, 1987), pp. 373–375.

[11] D. Y. K. Ko and J. C. Inkson, Phys. Rev. B **38**, 9945 (1988).

[12] Equation (3.9) is the generalized equivalent of the standard orthogonality condition for symmetric matrices. See, for example, B. N. Parlett, *The Symmetric Eigenvalue Problem* (Prentice-Hall, Englewood Cliffs, NJ, 1980) Chap. 1.

[13] If the dipole is at the interface between nonidentical layers, $\hat{\eta}$ is replaced by the average of its values in the two layers.

[14] LAPACK routines, available from http://www.netlib.org/lapack/, were used for the numerical results presented here.

[15] See, for example, *Handbook of Applied Mathematics*, 2nd ed., edited by C. E. Pearson (Van Nostrand Reinhold, New York, 1990), p. 888.

[16] K. M. Ho, C. T. Chan, and C. M. Soukoulis, Phys. Rev. Lett. **65**, 3152 (1990); R. D. Meade, A. M. Rappe, K. D. Brommer, J. D. Joannopoulos, and O. L. Alerhand, Phys. Rev. B **48**, 8434 (1993).

[17] J. T. Boyd, IEEE J. Quantum Electron. **8**, 788 (1972).

[18] D. Cassagne, C. Jouanin, and D. Bertho, Phys. Rev. B **53**, 7134 (1996).